ACS APPLIED MATERIALS & INTERFACES

Research Article

www.acsami.org

Enhanced Photovoltaic Properties of Nb_2O_5-Coated TiO_2 3D Ordered Porous Electrodes in Dye-Sensitized Solar Cells

Hye-Na Kim and Jun Hyuk Moon*

Department of Chemical and Biomolecular Engineering, Sogang University, Seoul 121-742, South Korea

Supporting Information

ABSTRACT: This paper describes the use of Nb_2O_5-coated TiO_2 3D ordered porous electrodes in dye-sensitized solar cells. We employed bilayer inverse opal structures as a backbone of 3D porous structures, and the number of Nb_2O_5 coatings was controlled, determining the concentration of Nb_2O_5 coating. XPS measurements confirmed the formation of Nb_2O_5. The uniformity of the Nb_2O_5 coating was characterized by elemental mapping using SEM and TEM measurements. Photovoltaic measurement on dye-sensitized solar cells (DSSCs) that incorporated Nb_2O_5/TiO_2 inverse opal electrodes yielded a maximum efficiency of 7.23% for a 3.3 wt % Nb_2O_5 coating on a TiO_2 IO structure. The Nb_2O_5 significantly increased the short-circuit current density (J_{SC}). Electrochemical impedance spectroscopy was used to measure the J_{SC}, revealing an enhanced electron injection upon deposition of the Nb_2O_5 coating.

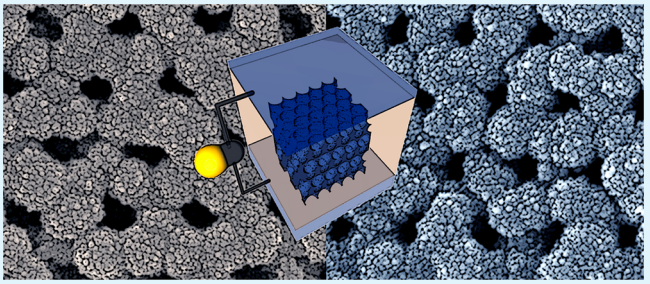

KEYWORDS: *photoelectrodes, inverse opals, metal oxide coating, dye-sensitized solar cells, niobium oxide*

INTRODUCTION

Dye-sensitized solar cells (DSSCs) are promising alternatives to conventional silicon-based solar cells because of their low manufacturing costs and relatively high energy conversion efficiencies.[1] In DSSC components, the TiO_2 electrode layer is a key part because this layer performs many functions: it acts as a substrate on which the dye molecules adsorb, it transfers the charges, and it serves as a diffusion pathway for redox ions. The engineering of TiO_2 electrodes with regard to characteristics such as nanostructure, crystalline morphology, and surface properties is therefore a crucial aspect of efforts to enhance the photoconversion efficiency. There have been many efforts to engineer the microstructure of TiO_2 electrodes. It is thought that control over the meso-to-macroscale morphology of an oxide semiconductor film could increase the efficiency of DSSCs.[2,3] Moreover, this could be required for the application of highly viscous electrolytes in solid-state DSSCs. Recently, ordered morphologies, such as nanotube arrays,[4−7] ordered mesoporous structures,[8,9] and inverse opals[10,11] have been suggested and widely studied.

Inverse opal (IO) electrodes containing three-dimensional bicontinuous porous structures and pores recently have raised interest due to the following reasons.[11−15] (1) As with other ordered morphologies, the 3D connected structures of IO coatings provide more direct transport route for electrons. (2) The pore size can be widely tuned by varying the colloidal crystal template particle size. Fully connected pores provide superior penetration of hole conductors, particularly in solid-state DSSCs. (3) Colloidal templating approaches allow the facile engineering of multilayered structures. For example, the electron mobility and the charge recombination properties were much enhanced by using a strategy in which TiO_2/Al/ZnO TiO_2/SnO_2 inverse opal-like core−shell structure were prepared. These coatings yielded large increases in the photovoltage of 15% over a state-of-the−art DSSC and provided higher efficiencies of 5.8% by using Z907 and I_3^-/I^- electrolyte.[12] However, IO-based electrodes revealed a much lower short-circuit current density (J_{SC}), in the range of 10−12 mA/cm^2 compared to the J_{SC} measured for state-of-the-art DSSCs.[16] Thus, the J_{SC} of IO-based electrodes must be enhanced.

The J_{SC} values of DSSCs with TiO_2 electrodes are determined by three factors, the light harvesting efficiency, the electron injection efficiency, and the electron collection efficiency. The light harvesting efficiency may be increased by increasing light absorption through dye loading or scattering. Previously, our group reported the preparation of bilayer TiO_2 inverse opals in which the inverse opal surface was covered by rutile TiO_2 nanoparticles that increased the specific area of the electrode for dye loading, thereby enhancing the photocurrent density. These electrodes yielded high efficiencies of 4.6% by using unpurified N719 and I_3^-/I^- electrolyte.[14] Meanwhile, the injection and collection efficiencies may be increased by modulating the surface states of the TiO_2 electrodes.[2] Previous studies have examined the application of various metal oxide shells such as SnO_2,[17] ZrO_2,[18] Nb_2O_5,[19−22] Al_2O_3,[18,23,24] and

Received: July 25, 2012
Accepted: November 7, 2012
Published: November 15, 2012

   dx.doi.org/10.1021/am3014554 | ACS Appl. Mater. Interfaces 2012, 4, 5821−5825

ZnO[25,26] to TiO_2 electrodes. Mostly, the coating of these materials layer forms an energy barrier that decreases the electron recombination losses, shifts the conduction band downward that increases the electron injection, or enhances the injection efficiency. This results in an increase in the J_{SC} and often accompanies the increase in open-circuit voltage (V_{OC}) as well. Here, we employed a Nb_2O_5 coating on TiO_2 IO structures for use in DSSCs. Nb_2O_5 is such a promising metal oxide because it supports good N719 dye loading because of its basic character and its conduction band level is 100 meV higher than that of TiO_2.[22] In measuring the photovoltaic performances, the J_{SC} largely increased by up to 60% from 10.45 to 16.73 mA/cm^2, therefore, the photon-to-electric conversion efficiency increased by 46% from 4.95% to 7.23% (using nonpurified N719). It should be noted that this remarkable improvement was superior to previous results employing Nb_2O_5 coatings on nanocrystalline TiO_2 electrodes[21,27] and TiO_2 nanorods.[19]

EXPERIMENTAL SECTION

Fabrication of IO TiO_2 Electrodes. The FTO substrate was washed thoroughly and a thin layer of TiO_2 was deposited as a blocking layer, as reported elsewhere. A layer of monodisperse polystyrene (PS) particles 750 nm in diameter was coated onto the FTO substrates and assembled during the evaporation of water. TiO_2 nanoparticles with an average size of 15 nm (NanoAmor Inc.) were dispersed in water and applied to the PS particle layer, into which they infiltrated. The PS-TiO_2 composite film was calcined in air at 500 °C for 2 h, leaving behind an inverse opal structure. The sample was post-treated in an aqueous 0.3 M $TiCl_4$ solution to enhance the surface roughness with a coating of rutile TiO_2 nanoparticles. In this work, the post-treated inverse opal will be referred to as IO TiO_2.

Nb_2O_5 Coating on the IO TiO_2 Electrodes. The Nb_2O_5 precursor solution was prepared from a 0.02 M $NbCl_5$ (Sigma-Aldrich) solution in anhydrous ethanol. The solution was dropped onto the IO TiO_2 layer and spin-coated to remove residual precursor solution. The total Nb_2O_5 coating thickness was modulated by the number of coatings applied. Finally, the substrate was sintered at 500 °C for 30 min to complete the conversion into a crystallized Nb_2O_5 layer.

Assembly of the DSSCs. The IO TiO_2 layer was dipped for 20 h in a dye solution containing 0.5 mM N719 (Dyesol) dye. Subsequently, an active area of the TiO_2 electrode was formed by scraping. The surface areas were 9 - 10 mm^2. The counter electrode was prepared by coating a 0.7 mM H_2PtCl_6 solution in anhydrous ethanol onto the FTO substrate. After then, the TiO_2 electrode was assembled with the counter electrode, and the gap between the two electrodes was fixed using a 60 μm thick polymeric film (Surlyn, DuPont). The, the electrolyte solution was injected into the gap. The electrolyte solution contained 0.05 M LiI (Sigma-Aldrich), 0.1 M guanidine thiocyanate (GSCN) (Wako), 0.03 M I_2 (Yakuri), 0.5 M 4-tert-butylpyridine (Aldrich), and 0.7 M 1-butyl-3-methylimidazolium iodide (BMII) (Sigma-Aldrich) in a solution containing acetonitrile (Aldrich) and valeronitrile (85:15 v/v).

Characterization. The surface morphologies of the inverse opals and the Nb_2O_5-coated TiO_2 inverse opals were investigated using scanning electron microscopy (SEM, Carl Zeiss). The atomic concentrations of Nb_2O_5 were measured by energy dispersive X-ray spectroscopy (EDX) in conjunction with the SEM measurements. Elemental mapping of the Nb_2O_5-coated TiO_2 IO structure was performed using transmission electron microscopy (TEM, JEOL). The binding energy of the Nb_2O_5 coating surface was measured by X-ray photoelectron spectroscopy (XPS, Thermo Fisher Scientific). The photocurrents and voltages of the DSSCs were measured using a Source Meter (Keithley Instruments) under simulated solar light produced using a 150 W Xe lamp (Peccell) and AM 1.5G filters without masking. The intensity was adjusted using a Si reference cell (BS-520, Bunko-Keiki) to a power density of 100 mW cm^{-2}. The electrochemical impedance spectra were measured using a potentiostat (Versastat, AMETEK). The frequency range explored in the impedance measurements was 1×10^5 to 0.5 Hz.

RESULTS AND DISCUSSION

Figure 1 shows SEM images of the IO TiO_2 without Nb_2O_5 and Nb_2O_5-coated IO TiO_2. The IO TiO_2 was prepared by using PS colloidal crystal templates (see Figure S1a in the Supporting Information). The Nb_2O_5 coating was characterized by XPS measurements, which confirmed the chemical structure. An extended post-treatment of $TiCl_4$ precursor solution was applied to increase the surface area of the inverse opal structure (see Figure S1b in the Supporting Information) by growing TiO_2 nanoparticles (15−20 nm sized), as reported elsewhere.[14] The inverse opal possessed ordered pores around 250 nm in diameter, as shown in Figure 1a. Figure 1b shows that the Nb_2O_5 layer coating was not visible in the SEM images because of the thinness of the layer.

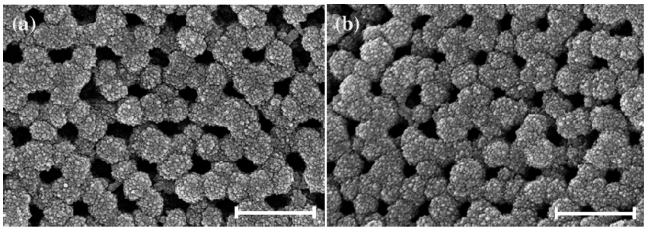

Figure 1. SEM images of the TiO_2 inverse opal structures of (a) bare IO TiO_2 and (b) 3.3 wt %-Nb_2O_5 IO TiO_2. (Scale bar: 1 μm).

The Nb_2O_5 coating layer was prepared from a 0.02 M precursor solution. Lower solution concentrations yielded thin nonreproducible coatings that were nearly unobservable under EDX measurements (20 kV). Figure 2 shows TEM images of the IO TiO_2 structures prepared from 3.3 wt %-Nb_2O_5 IO TiO_2 and the TEM elemental mappings. The results show that the Nb atoms were homogeneously coated onto the IO structures.

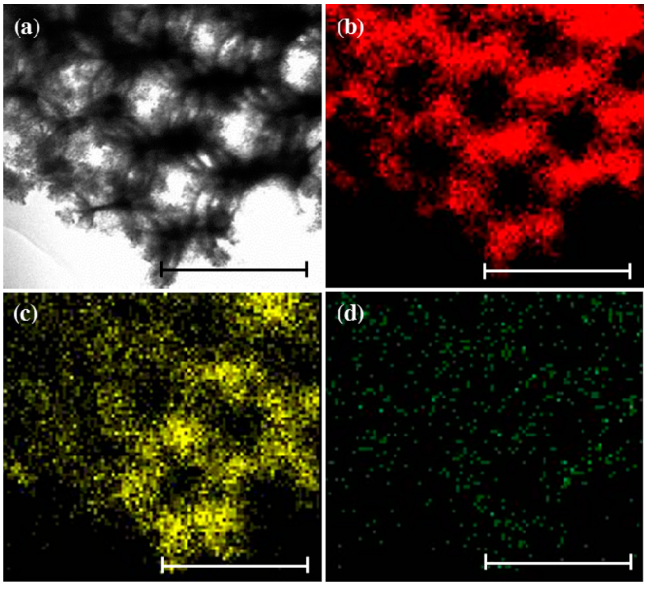

Figure 2. (a) TEM image of inverse opal structures of 3.3 wt %-Nb_2O_5 IO TiO_2 and the elemental mapping for (b) Ti, (c) O, and (d) Nb atoms (scale bar: 1 μm).

Electrodes were prepared with 1 and 3 coatings, yielding atomic wt % Nb values of 3.3 and 4.0, respectively (see Table 1S in the Supporting Information). The signature of Nb atoms in the EDX analysis did not guarantee the formation of Nb_2O_5; therefore, XPS measurements were collected to verify that the Nb atoms were present as Nb_2O_5 and not as other oxidized forms of Nb, such as NbO or NbO_2.

Figure 3 shows the XPS spectrum for the Nb precursor-coated IO TiO_2 electrodes. The highly oxophilic niobium can

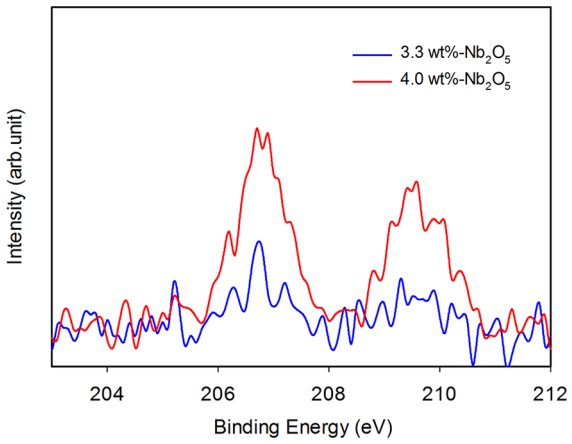

Figure 3. XPS investigation for the surface of TiO_2 electrode. Nb 3d spectra of Nb_2O_5-coated IO TiO_2 electrodes, for different atomic %.

produce niobium oxide in the forms of NbO, NbO_2, or Nb_2O_5 under an oxygen environment, rather than remaining as metallic Nb. The XPS spectral peaks correspond to the binding energies of the niobium oxide $3d_{3/2}$ and $3d_{5/2}$ electrons, which can be used to differentiate the oxides: 207 and 204 eV indicate NbO, 208 and 205 eV indicate NbO_2, and 210 and 208 eV indicate Nb_2O_5.[28] The major peaks were positioned at 207 and 210 eV, confirming the presence of Nb_2O_5. As the coating thickness increased, the peak intensity increased, as measured by EDX analysis.

The performances of the Nb_2O_5-coated IO TiO_2 electrodes were evaluated in DSSCs by sensitizing the electrodes in a 0.5 mM N719 dye solution, then assembling the electrodes with a Pt-coated counter electrode. The interelectrode gap was filled with a liquid electrolyte. The current−voltage (J−V) characteristics of the DSSCs prepared with electrodes coated with various wt% Nb_2O_5 were measured under 100 mW cm^{-2} AM 1.5 illumination. Figure 4 shows the J-V curves for DSSC cells containing untreated IO TiO_2 and Nb_2O_5-coated IO TiO_2 electrodes coated with various atomic wt% Nb_2O_5. Table 1 lists the J−V parameters extracted from the J−V curves, including the J_{SC}, V_{OC}, FF, and the overall conversion efficiency (η), calculated according to $J_{SC} \times V_{OC} \times FF/(100\ mW\ cm^{-2})$. The J_{SC} of the 3.3 wt %-Nb_2O_5 IO TiO_2 (16.73 mA cm^{-2}) was 60% higher than the J_{SC} of the untreated IO TiO_2 (10.45 mA cm^{-2}). This enhancement led to a 46% improvement in the conversion efficiency, which reached 7.23%. It should be noted that an efficiency of 7.23% is the highest efficiency yet achieved using inverse opal-type electrodes. We compared our maximum efficiency with the efficiencies of DSSCs containing conventional nanocrystalline TiO_2 electrodes of the same film thickness, which were prepared under the same experimental conditions as those used here (see Figure S2 in the Supporting Information). We obtained a 7.5% efficiency for these DSSCs,

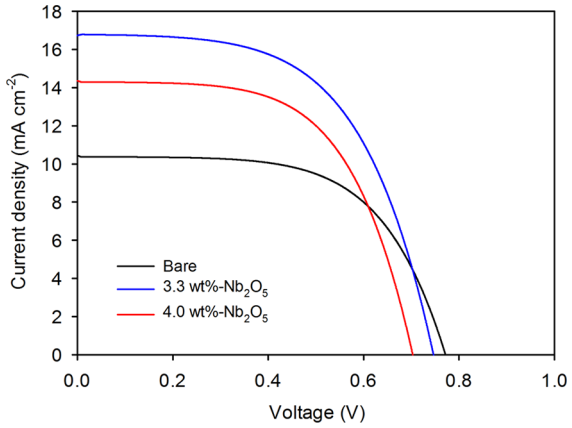

Figure 4. The current−density (J−V) curves for DSSC cells containing untreated IO TiO_2 and Nb_2O_5-coated IO TiO_2 electrodes, for different atomic %.

Table 1. Photovoltaic Parameters for DSSC cells Fabricated with Untreated IO TiO_2 and Nb_2O_5-Coated IO TiO_2 Electrodes, For Different Atomic % Tested under AM 1.5G 100 mW cm^{-2}

atomic wt % of coated Nb_2O_5	J_{sc} (mA cm^{-2})	V_{oc} (V)	FF	η (%)	R_{rec}(Ω)	C_μ (mF)
untreated	10.45	0.77	0.61	4.95	139.1	0.35
3.3	16.73	0.75	0.58	7.23	89.5	0.45
4.0	14.37	0.71	0.60	6.08	96.0	0.37

which was comparable to the efficiency of our maximum efficiency.

Here, the increase in J_{SC} (by 60%) observed in the IO TiO_2 electrodes was more dramatic than the average enhancements in J_{SC} reported previously. Previous studies of the Nb-doped nanocrystalline TiO_2 and TiO_2 electrodes reported J_{SC} enhancements of up to 50% relative to untreated electrodes.[19,21,27] This enhancement may be attributed to the relative uniformity of the Nb_2O_5 coating through the fully connected pores in the IO structure. Coatings with other morphologies presented nonuniform pore networks or small pore sizes.

The J−V graphs obtained under front-side or back-sided illumination conditions were compared, as shown in Figure 5. Front-side and back-side illumination generated more electrons,

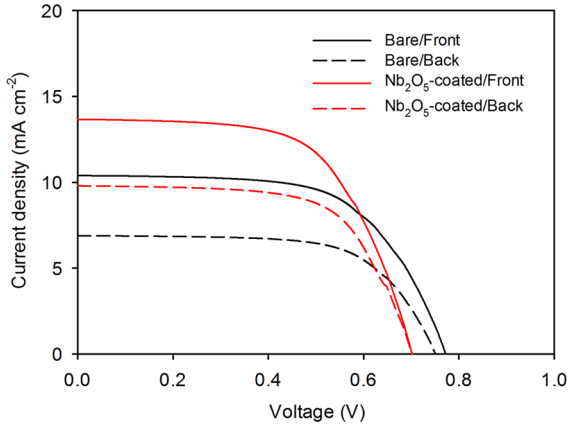

Figure 5. The current−density (J−V) curves for DSSC cells containing untreated IO TiO_2 and Nb_2O_5 IO TiO_2 in front-sided illumination and back-sided illumination condition.

dx.doi.org/10.1021/am3014554 | ACS Appl. Mater. Interfaces 2012, 4, 5821−5825

respectively, near and far from the electron collecting substrate. The electrons generated under back-side illumination (through the Pt-coated counter electrode) experienced a large number of trapping/detrapping events (trap-limited transport), which delayed the electron transport time and increased the charge recombination rate. In front-side illumination, electrons near the collecting substrate increased the conductivity of TiO_2, which facilitated rapid trap-free transport.[29] Thus, the relative values of J_{SC} under back-side and front-side illumination provided qualitative information about the electron recombination and transport properties of TiO_2 electrodes. A comparison of DSSCs prepared with untreated IO TiO_2 electrodes or Nb_2O_5-coated IO TiO_2 electrodes, which displayed comparable J_{SC} values, showed that the back-to-front-side illumination J_{SC} ratios were 34% for the untreated IO TiO_2 electrodes and 28% for the Nb_2O_5-coated IO TiO_2 electrodes. The Nb_2O_5 coating clearly suppressed the reduction in J_{SC} under back-side illumination, suggesting that the coating reduced the recombination reaction or simply increased the conductivity of the TiO_2 electrodes due to more injected electrons.

We further investigated the dramatic increase in J_{SC} for DSSCs prepared with increasing Nb_2O_5 in the Nb_2O_5-coated electrodes by comparing the 3.3 wt %-Nb_2O_5 electrode to the uncoated sample. Electrochemical impedance spectroscopy (EIS) was used to characterize the electron transport in the Nb_2O_5-coated IO TiO_2 electrodes by comparison with the untreated IO TiO_2 electrode, as shown in Figure 6. In Figure 6,

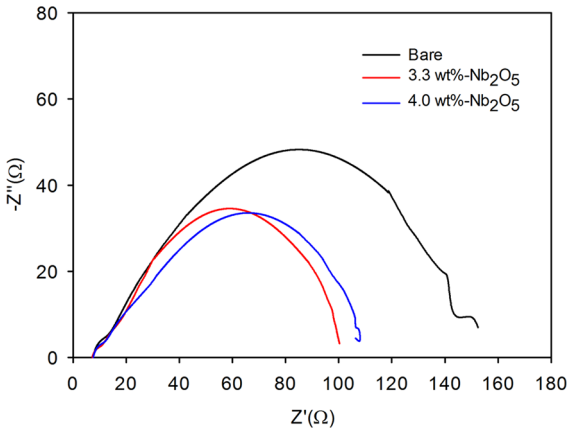

Figure 6. Electrochemical impedance spectroscopy (EIS) under illumination condition for DSSC cells containing untreated IO TiO_2 and Nb_2O_5-coated IO TiO_2, for different atomic %.

the Nyquist plot revealed a large semicircle in the frequency range between 1 kHz and 1 Hz. The size of the arc depended on the concentration of I_3^- and on the rate of back-electron transfer at the TiO_2/electrolyte interface. The impedance spectrum was analyzed using an equivalent circuit for the TiO_2/electrolyte interface in the conductive state. The recombination resistance (R_{rec}) was obtained by the curve of the large semicircle, as reported elsewhere.[30] In Table 1, the value of R_{rec} decreased from 139.1Ω for the untreated electrode to 89.5 Ω for the 3.3 wt %-Nb_2O_5 IO TiO_2 electrodes, which was a 36% decrease upon introduction of the Nb_2O_5 coating. This implies that the coating is not forming a barrier layer to reduce the recombination loss. Meanwhile, the chemical capacitance (C_μ) was also estimated as listed in Table 1. The chemical capacitance describes the density of states in the bandgap of TiO_2.[31] the value of C_μ for the Nb_2O_5-coated sample was 0.045 F, which was 29% higher than the value of 0.35mF for the untreated sample. Moreover, a lowered degree of dye adsorption was observed on the Nb_2O_5-coated electrodes (0.033 μmol cm^{-2} for 3.3 wt %-Nb_2O_5 IO TiO_2) compared to the amount of dye adsorbed onto the untreated TiO_2 electrode (0.057 μmol cm^{-2}). The number of electrons generated by the adsorbed dye molecules on the Nb_2O_5-coated TiO_2 surface was not higher. Thus, our results imply that the enhancement in the electron injection of TiO_2 electrodes due to the Nb_2O_5 coating improves the J_{SC} value.

The enhancement of the electron injection might be attributed to the shift of conduction band edge of TiO_2. Previously, it has been reported that the acidic property of Nb_2O_5 shifted the TiO_2 flat band energy potential (E_{fb}) toward positive values and increased the driving force for electron injection (determined as the difference between E_{fb} and the LUMO state of the dye), thereby enhancing the electron injection efficiency.[18] Here, in Figure 7, we measured the cyclic

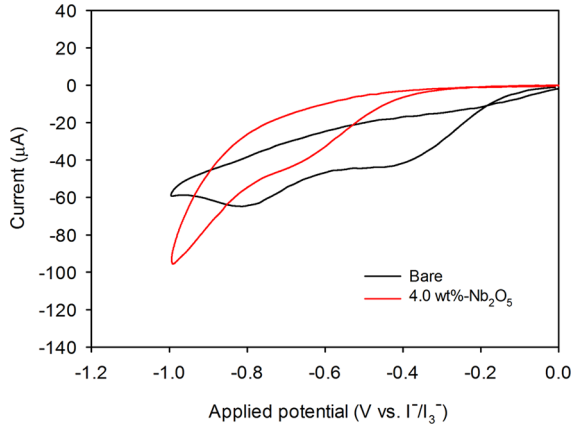

Figure 7. Cyclic voltammetry for the untreated IO TiO_2 and 4.0 wt %-Nb_2O_5 IO TiO_2 electrode in the I_3^-/I^- electrolyte.

voltammetry curves of the bare and Nb_2O_5-coated TiO_2 electrodes in the obtained in the electrolyte solution of 0.05 M LiI, 0.003 M I_2 under the scanning range of −1 V to 0 (versus I_3^-/I^-). The cyclic voltammetry is sensitive to the interfacial electron flow in the electrode/electrolyte interface.[32,33] The voltammetric curves show the reduction peaks attributed to the charging/discharging at the interface and the peak was shifted positively upon the Nb_2O_5 coating. This result confirms the positive shift of the conduction band edge in Nb_2O_5-coated IO TiO_2 electrodes.

Meanwhile, the J_{SC} value observed for thick (greater than 3.3 wt %) Nb_2O_5 coatings decreased by as much as 14% relative to 3.3 wt %-Nb_2O_5 IO TiO_2 electrode, which decreased η. The DSSCs prepared here using Nb_2O_5-coated IO TiO_2 electrodes displayed enhanced J_{SC} and η values compared to the untreated IO-TiO_2 electrodes. The thicker Nb_2O_5 coating slightly increased the recombination resistance, R_{rec}, but the capacitance C_μ was decreased. This implies that the thicker Nb_2O_5 coating might not further shift the conduction band but rather impair the electron injection because of the increase in injection resistance itself.

CONCLUSION

We investigated Nb_2O_5-coated TiO_2 inverse opal electrodes for use in highly efficient DSSCs. The presence of Nb_2O_5 in the

coating, prepared via the oxidation of a hydrated $NbCl_5$ precursor, was confirmed by XPS measurements. The uniformity of the Nb_2O_5 coatings was achieved by preparing a fully connected porous IO structure, as confirmed by EDX analysis. The photovoltaic performances of the Nb_2O_5 coating on the TiO_2 inverse opal electrodes showed that J_{SC} increased by up to 60%, from 10.45 to 16.73 mA/cm^2. The photon-to-electric conversion efficiency was thereby increased by 46%, from 4.95% to 7.23%. The $J-V$ graphs obtained under front-side or back-sided illumination conditions were compared. The Nb_2O_5 coating clearly suppressed the reduction in J_{SC} under back-side illumination. The EIS analysis revealed a large increase in the chemical capacitance, thereby the electron injection efficiency upon introduction of the Nb_2O_5 coating. The maximum efficiency of 7.23% observed here is the highest efficiency yet reported for inverse opal-based electrodes. Our approach demonstrates a simple route to enhancing the J_{SC} and, thereby, the efficiency of DSSCs employing inverse opal electrodes.

■ ASSOCIATED CONTENT

Ⓢ Supporting Information

SEM images and transmission spectra. This information is available free of charge via the Internet at http://pubs.acs.org.

■ AUTHOR INFORMATION

Corresponding Author

*E-mail: junhyuk@sogang.ac.kr.

Notes

The authors declare no competing financial interest.

■ ACKNOWLEDGMENTS

This work was supported by the National Research Foundation of Korea (2011-0030250). The Korea Basic Science Institute is also acknowledged for SEM, TEM and XPS measurements.

■ REFERENCES

(1) Oregan, B.; Gratzel, M. *Nature* **1991**, *353*, 737−740.
(2) Hagfeldt, A.; Boschloo, G.; Sun, L. C.; Kloo, L.; Pettersson, H. *Chem. Rev.* **2010**, *110*, 6595−6663.
(3) Wang, Z. S.; Kawauchi, H.; Kashima, T.; Arakawa, H. *Coord. Chem. Rev.* **2004**, *248*, 1381−1389.
(4) Zhang, Z. H.; Yu, Y. J.; Wang, P. *ACS Appl. Mater. Interfaces* **2012**, *4*, 990−996.
(5) Zhuge, F. W.; Qiu, J. J.; Li, X. M.; Gao, X. D.; Gan, X. Y.; Yu, W. D. *Adv. Mater.* **2011**, *23*, 1330−1334.
(6) Zheng, Q.; Kang, H.; Yun, J.; Lee, J.; Park, J. H.; Baik, S. *ACS Nano* **2011**, *5*, 5088−5093.
(7) Pan, X. A.; Chen, C. H.; Zhu, K.; Fan, Z. Y. *Nanotechnology* **2011**, *22*, 235402.
(8) Sauvage, F.; Chen, D. H.; Comte, P.; Huang, F. Z.; Heiniger, L. P.; Cheng, Y. B.; Caruso, R. A.; Graetzel, M. *ACS Nano* **2010**, *4*, 4420−4425.
(9) Zukalova, M.; Zukal, A.; Kavan, L.; Nazeeruddin, M. K.; Liska, P.; Gratzel, M. *Nano Lett.* **2005**, *5*, 1789−1792.
(10) Lee, S. H. A.; Abrams, N. M.; Hoertz, P. G.; Barber, G. D.; Halaoui, L. I.; Mallouk, T. E. *J. Phys. Chem. B* **2008**, *112*, 14415−14421.
(11) Kuo, C. Y.; Lu, S. Y. *Nanotechnology* **2008**, *19*, 095705.
(12) Tetreault, N.; Arsenault, E.; Heiniger, L. P.; Soheilnia, N.; Brillet, J.; Moehl, T.; Zakeeruddin, S.; Ozin, G. A.; Gratzel, M. *Nano Lett.* **2011**, *11*, 4579−4584.
(13) Guldin, S.; Huttner, S.; Kolle, M.; Welland, M. E.; Muller-Buschbaum, P.; Friend, R. H.; Steiner, U.; Tetreault, N. *Nano Lett.* **2010**, *10*, 2303−2309.
(14) Shin, J. H.; Moon, J. H. *Langmuir* **2011**, *27*, 6311−6315.
(15) Cho, C. Y.; Moon, J. H. *Adv. Mater.* **2011**, *23*, 2971−2975.
(16) Yella, A.; Lee, H. W.; Tsao, H. N.; Yi, C. Y.; Chandiran, A. K.; Nazeeruddin, M. K.; Diau, E. W. G.; Yeh, C. Y.; Zakeeruddin, S. M.; Gratzel, M. *Science* **2011**, *334*, 629−634.
(17) Prasittichai, C.; Hupp, J. T. *J. Phys. Chem. Lett.* **2010**, *1*, 1611−1615.
(18) Palomares, E.; Clifford, J. N.; Haque, S. A.; Lutz, T.; Durrant, J. R. *J. Am. Chem. Soc.* **2003**, *125*, 475−482.
(19) Barea, E.; Xu, X. Q.; Gonzalez-Pedro, V.; Ripolles-Sanchis, T.; Fabregat-Santiago, F.; Bisquert, J. *Energy Environ. Sci.* **2011**, *4*, 3414−3419.
(20) Ueno, S.; Fujihara, S. *Electrochim. Acta* **2011**, *56*, 2906−2913.
(21) Yang, M.; Kim, D.; Jha, H.; Lee, K.; Paul, J.; Schmuki, P. *Chem. Commun.* **2011**, *47*, 2032−2034.
(22) Ahn, K. S.; Kang, M. S.; Lee, J. K.; Shin, B. C.; Lee, J. W. *Appl. Phys. Lett.* **2006**, *89*, 013103.
(23) Lin, C.; Tsai, F. Y.; Lee, M. H.; Lee, C. H.; Tien, T. C.; Wang, L. P.; Tsai, S. Y. *J. Mater. Chem.* **2009**, *19*, 2999−3003.
(24) Makinen, V.; Honkala, K.; Hakkinen, H. *J. Phys. Chem. C* **2011**, *115*, 9250−9259.
(25) Law, M.; Greene, L. E.; Radenovic, A.; Kuykendall, T.; Liphardt, J.; Yang, P. D. *J. Phys. Chem. B* **2006**, *110*, 22652−22663.
(26) Roh, S. J.; Mane, R. S.; Min, S. K.; Lee, W. J.; Lokhande, C. D.; Han, S. H. *Appl. Phys. Lett.* **2006**, *89*, 253512.
(27) Lu, X. J.; Mou, X. L.; Wu, J. J.; Zhang, D. W.; Zhang, L. L.; Huang, F. Q.; Xu, F. F.; Huang, S. M. *Adv. Funct. Mater.* **2010**, *20*, 509−515.
(28) Kuznetsov, M. V.; Razinkin, A. S.; Shalaeva, E. V. *J. Struct. Chem.* **2009**, *50*, 514−521.
(29) Hsiao, P. T.; Liou, Y. J.; Teng, H. S. *J. Phys. Chem. C* **2011**, *115*, 15018−15024.
(30) Adachi, M.; Sakamoto, M.; Jiu, J. T.; Ogata, Y.; Isoda, S. *J. Phys. Chem. B* **2006**, *110*, 13872−13880.
(31) Barea, E. M.; Zafer, C.; Gultekin, B.; Aydin, B.; Koyuncu, S.; Icli, S.; Santiago, F. F.; Bisquert, J. *J. Phys. Chem. C* **2010**, *114*, 19840−19848.
(32) Kang, S. H.; Kim, J. Y.; Kim, Y.; Kim, H. S.; Sung, Y. E. *J. Phys. Chem. C* **2007**, *111*, 9614−9623.
(33) Saruwatari, K.; Sato, H.; Idei, T.; Kameda, J.; Yamagishi, A.; Takagaki, A.; Domen, K. *J. Phys. Chem. B* **2005**, *109*, 12410−12416.